M W Journal of Science
e-ISSN: 3023-770X
https://doi.org/10.5281/zenodo.19650482 MW Journal of Science, 2026, 3, 1, 7-17

High Temperature Oxidation Kinetics and Corrosion Parameters of Ti-25Nb-5Ta-2V and Ti-25Nb-5Ta-2Ni Alloys

Necdet Ercan[1], Esra Balcı[2], and Fethi Dağdelen[3]*

[1] Firat University, Faculty of Science, Department of Physics, 23200 Elazığ / TÜRKİYE
[2] Hatay Mustafa Kemal University, Kırıkhan Vocational School, Department of Optician, Hatay / TÜRKİYE
[3] Firat University, Faculty of Science, Department of Physics, Elazig 23119 / TÜRKİYE
*Corresponding author: fdagdelen@firat.edu.tr

Abstract

In this study, high-temperature oxidation behavior and electrochemical corrosion properties of Ti-25Nb-5Ta-2V (TNTV) and Ti-25Nb-5Ta-2Ni (TNTN) alloys performed. Thermogravimetric analyses indicated that both alloys exhibit mass gain with increasing temperature, attributable to the formation of oxide layers. The TNTV alloy demonstrated a more pronounced oxidation rate, which is ascribed to the elevated oxidative reactivity of vanadium. Electrochemical evaluations, including potentiodynamic polarization and electrochemical impedance spectroscopy (EIS), revealed that TNTN possesses superior corrosion resistance in a simulated seawater, as evidenced by higher polarization resistance and charge transfer resistance relative to TNTV. These results highlight the significant influence of alloying elements on oxidation kinetics and corrosion mechanisms, indicating enhanced electrochemical stability of TNTN relative to TNTV.

Keywords: High-temperature oxidation, Electrochemical corrosion, Polarization resistance, Titanium alloys

Introduction

Titanium and titanium-based alloys possess a wide range of applications, extending from biomedical implants to the aerospace industry, owing to their low density, high specific strength, and excellent biocompatibility [1, 2]. These alloys undergo significant changes in their phase transformation temperatures and mechanical properties as a result of applied heat treatments [3, 4]. One of the most critical factors determining the long-term performance of these materials is their oxidation behaviour at elevated temperatures and their corrosion resistance in aggressive environments (e.g., seawater). High-temperature oxidation leads to the formation of either protective or permeable oxide layers on the material surface [5]; the structure and stability of these layers strongly depend on the type and concentration of alloying elements [6].

Niobium (Nb) and tantalum (Ta) act as β-phase stabilizers in titanium alloys, thereby enhancing oxidative stability at elevated temperatures. In contrast, vanadium (V) and nickel (Ni) exhibit distinct oxidation behaviours: vanadium readily oxidizes to form volatile oxides such as V_2O_5, whereas nickel can form a more stable NiO layer on the surface, providing a barrier effect against oxidation [7]. Therefore, a comparative investigation of Ti–Nb–Ta–V (TNTV) and Ti–Nb–Ta–Ni (TNTN) alloys is of significant importance for understanding oxidation kinetics and corrosion mechanisms.

In this study, the high-temperature oxidation behaviours of TNTV and TNTN alloys were investigated using TG/DTA analyses; additionally, corrosion parameters in a seawater environment were determined by employing potentiodynamic polarization and electrochemical impedance spectroscopy (EIS) techniques. Thermogravimetric analyses revealed mass gain and oxide layer formation in both alloys with increasing temperature. Electrochemical tests demonstrated that the TNTN alloy exhibits superior corrosion resistance compared to TNTV, owing to its higher polarization resistance and charge transfer resistance. Therefore, this study highlights the critical influence of alloying elements on oxidation and corrosion mechanisms in titanium-based alloys and contributes to the development of next-generation high-performance materials.

2. Material and Methods

The alloying elements Ti, Nb, Ta, Ni, and V (~99.8% purity) were weighed according to the compositions listed in Table 1 and homogeneously mixed using a mechanical mixer in powder form. The mixed powders were then compacted into disc-shaped samples with a diameter of 13 mm, as shown in Figure 1, by applying a pressure of approximately 1×10^6 Pa. The metal discs were subsequently alloyed via melting in an arc-melting furnace.

For TG/DTA analyses, specimens with approximate dimensions of $2 \times 2 \times 1.5$ mm³ were sectioned; their surface roughness removed, and cleaned using an ultrasonic cleaner. Thermogravimetric measurements were performed using a PerkinElmer Pyris TG/DTA instrument. The TG analysis was conducted by heating the samples from room temperature (RT) to 1000 °C at a rate of 20 °C/min. To investigate isothermal oxidation behaviour, separate samples were exposed to air at 500 °C, 750 °C, and 1000 °C for 80 minutes, during which mass gains due to oxidation were recorded.

Potentiodynamic corrosion tests were performed at room temperature in a simulated seawater solution prepared by dissolving 35 g of NaCl in 1.0 L of deionized water, using a Gamry Interface 1010 B potentiostat.

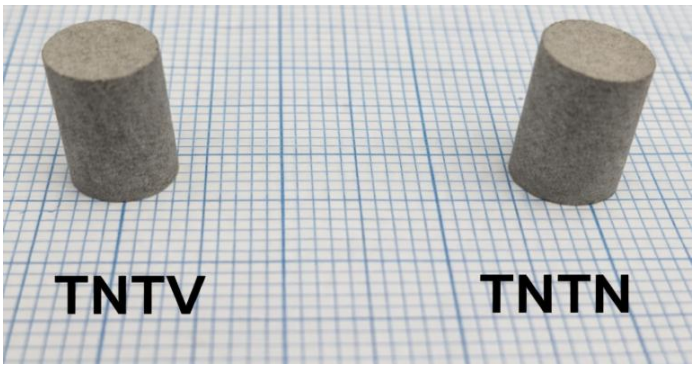

Figure 1. Pressed metal powders

Table 1. Atomic and mass composition ratios of the produced alloys.

Sample	Ti (at.%)	Nb (at.%)	Ta (at.%)	V (at.%)	Ni (at.%)
TNTV	68	25	5	2	0
TNTN	68	25	5	-	2

Results and Discussion

Figure 2 presents the thermogravimetric (TG) analysis of the samples conducted from room temperature up to 1000 °C. As observed from the graph, the mass of both samples exhibits an increasing trend up to 1000 °C. At lower temperatures (0–500 °C), the mass change follows an approximately linear increase. Beyond ~500 °C, the mass gain transitions to a parabolic behavior, which is likely associated with the acceleration of oxidation reactions occurring on the sample surface. The pronounced mass increase observed above 900 °C indicates the thickening of the oxide layer and the formation of new oxide phases[8]. This behavior also suggests that the material is capable of forming a protective oxide film under high-temperature oxidative conditions.

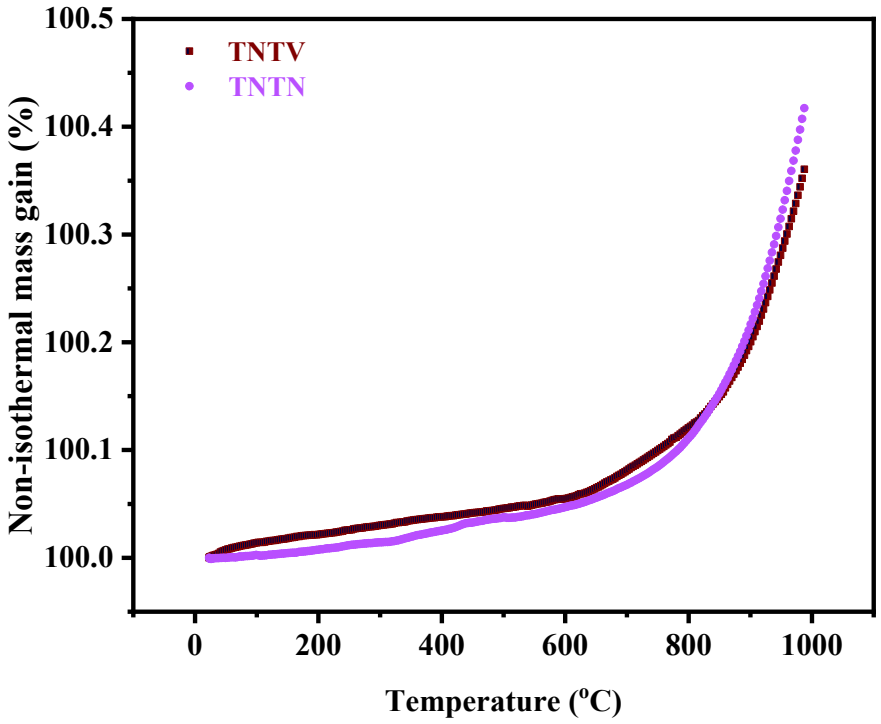

Figure 2. Thermogravimetric measurement results of the samples from room temperature to 1000 °C.

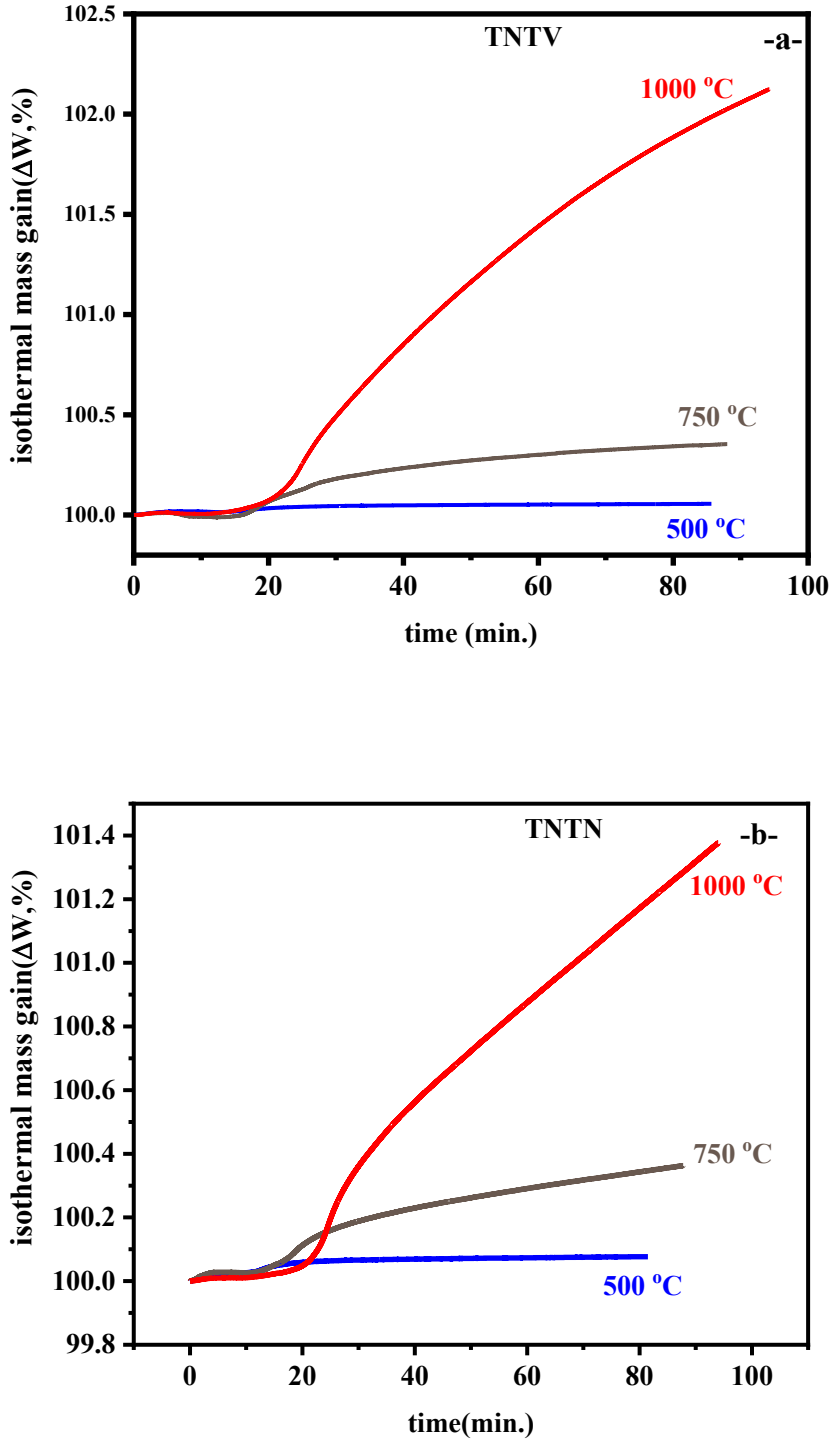

Figure 3. Graph of the time-dependent change of mass gain (ΔW) in air at 500 °C, 750 °C and 1000 °C for samples a) TNTV alloy, b) TNTN alloy.

Figures 3a and 3b illustrate the time-dependent mass gain of the alloys at 500 °C, 750 °C, and 1000 °C. This increase in mass is generally attributed to oxidation processes and the formation of oxide layers on the surface. For both samples, the negligible mass change observed at 500 °C indicates that the oxidation

rate is very slow at low temperatures. In contrast, both TNTV and TNTN samples exhibit a significant mass increase during 80 minutes of isothermal exposure at 750 °C and 1000 °C. When the two samples are compared, the TNTV specimen reaches higher values of isothermal oxidation rate. This behavior may be attributed to the higher reactivity of vanadium compared to nickel. Vanadium oxidizes more readily in air, forming oxides such as vanadium(V) oxide, whereas nickel tends to form a protective nickel(II) oxide layer on the surface[1], resulting in more stable oxidation behavior.

The thermal oxidation rate constant (k_p) of these alloys can be calculated using the following equation[5, 9, 10]:

$$\left(\frac{\Delta W}{\Delta A}\right)^2 = k_P \cdot t \quad (1)$$

$$k_p = k_o . \exp\left(E_o/RT\right) \quad (2)$$

Here, (ΔW/A) represents the mass gain per unit surface area, $\boldsymbol{t}$ denotes time, and $\boldsymbol{k_p}$ is the thermal oxidation rate constant. If the graph of $(\Delta W/A)^2$ against t is plotted, k can be calculated. Using the calculated k_p values, the activation energy (E_o) required for thermal oxidation was obtained from Equation 2 and is presented in Table 2. In this context, *T* represents the temperature and *R* is the universal gas constant (8.3144 kJ/mol).

An examination of the thermal oxidation kinetics obtained from TG analysis in Table 2 reveals a significant difference between the activation energies of the alloys. The activation energy of the TNTV alloy was calculated as 55.01 kJ·mol^{-1}, whereas that of the TNTN alloy was determined to be 67.72 kJ·mol^{-1}. A higher activation energy indicates that greater energy is required for the oxidation reaction to proceed, implying enhanced resistance of the material to oxidation.

In this context, the higher activation energy of the TNTN alloy compared to TNTV suggests that it exhibits more stable behavior against oxidation at elevated temperatures. Furthermore, the larger energy barrier for oxide formation in the TNTN alloy implies that the resulting oxide film may be more protective and stable.

Table 2. Calculated kp and activation energy values of the alloys.

Sample	Oxidation temperature (°C)	k_p (mg·cm^{-2}s^{-1})	Activation Energy (kJ·mol^{-1})
TNTV	500	$0.125 \cdot 10^{-2}$	55.01
	750	$5.059 \cdot 10^{-2}$	
	1000	1.120	
TNTN	500	$0.031 \cdot 10^{-2}$	67.72
	750	$2.026 \cdot 10^{-2}$	
	1000	1.473	

Figure 4 presents the Tafel curves obtained from potentiodynamic polarization measurements of the samples in a seawater environment. For the TNTV alloy, the corrosion potential (E_{corr}) was determined as −396.60 mV, the corrosion current density (i_{corr}) as 0.248 μA·cm^{-2}, the anodic Tafel slope (β_a) as 8.285

mV/dec, the cathodic Tafel slope (β*c*) as 6.428 mV/dec, and the corrosion rate (C_r) as 8.252 × 10^{-3} mm/year.

Examination of the potentiodynamic polarization curve of the TNTN sample shows that the corrosion potential is E_{corr} = −433 mV, indicating that the sample exhibits relatively active electrochemical behavior in the test environment. The corrosion current density obtained from the extrapolation of the anodic and cathodic Tafel regions (i_{corr} = 1.144 μA·cm^{-2}) suggests a low-to-moderate corrosion rate. The relatively high anodic Tafel slope (β_a = 361.40 mV/dec) indicates a deviation from classical Tafel behavior, likely influenced by factors such as passive film formation, instability of the surface oxide layer, or IR drop. In contrast, the cathodic slope (β*c* = 145.60 mV/dec) exhibits a more typical kinetic behavior. Additionally, the c corrosion rate (C_r) for TNTN was determined to be 1.703 × 10^{-2} mm/year.

Using these parameters, the polarization resistance (R_p) was calculated based on the Stern–Geary equation. The Stern–Geary constant (*B*) was determined using the following equation[6, 7, 11]. For the TNTV alloy,

$$B = \frac{\beta a \cdot \beta c}{2{,}303 \cdot (\beta a + \beta c)} \quad (3)$$

From this, the polarization resistance (R_p) can be determined as follows:

$$R_P = \frac{B}{\text{İ}coor} = \frac{0{,}001572}{2{,}488\ x\ 10^{-4}} \approx 6.32\ \Omega.cm^2 \quad (4)$$

It is calculated accordingly. The relatively high corrosion current density and the low polarization resistance indicate that the TNTV sample exhibits poor corrosion resistance. Furthermore, the obtained corrosion rate corresponds to a relatively stable condition (Very stable = 1.10^{-3}–1.10^{-2} mm/year) [11]. For the TNTN sample, the corrosion resistance calculated using the Stern–Geary relationship was determined as R_p = 39.39 kΩ·cm^2. This value suggests that the TNTN sample exhibits a certain degree of protection/passivation tendency in the solution; however, it does not possess a polarization resistance as high as that of a fully passive material. The obtained results are summarized in Table 3.

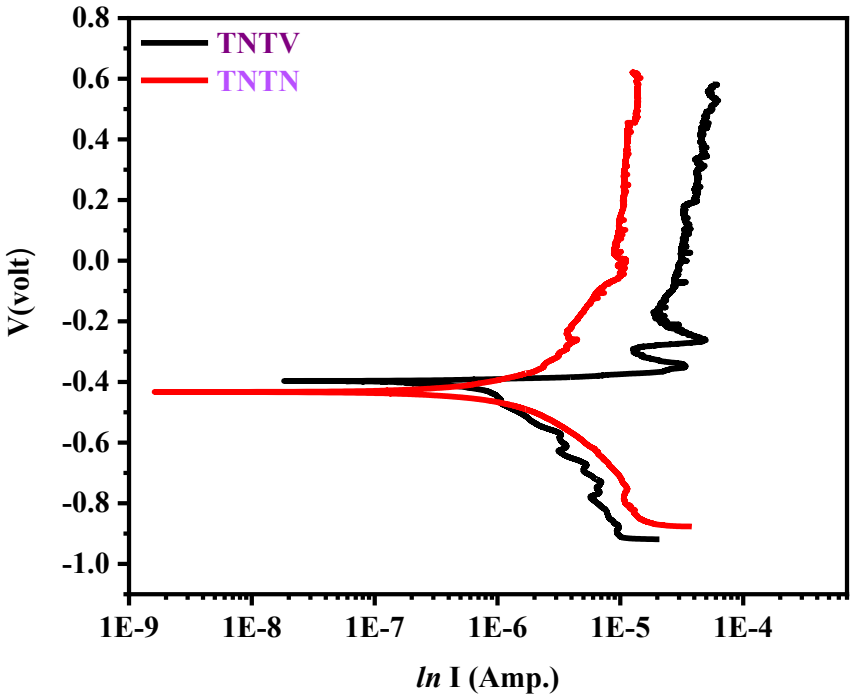

Figure 4. Tafel graph of the samples in % 3.5 NaCl.

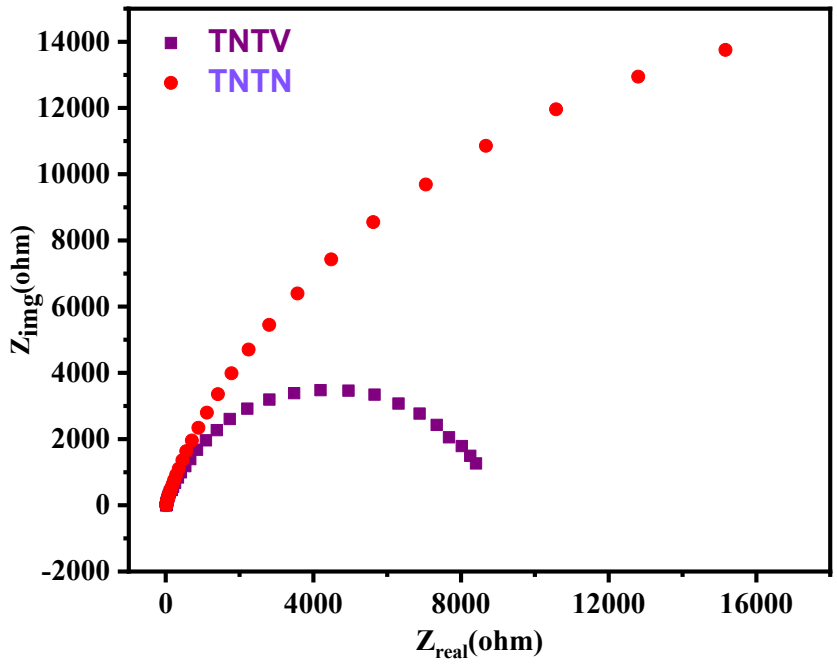

Figure 5. EIS Nyquist curves of the TNTV and TNTN samples.

The Nyquist diagram presented in Figure 5 illustrates the electrochemical impedance behavior of the TNTV and TNTN samples. The TNTV sample exhibits a distinct semicircular response in the low- and mid-frequency regions, indicating a relatively limited charge transfer resistance and the occurrence of comparatively faster electrochemical reactions at the surface.

In contrast, the TNTN sample shows a tendency extending toward higher $Z_{(real)}$ and $Z_{(imag)}$ values, suggesting higher overall impedance and the presence of more pronounced diffusion-controlled processes within the system. The larger radius of the Nyquist semicircle for the TNTN sample indicates a higher charge transfer resistance and implies that the surface layer formed acts as a more effective barrier against electrochemical reactions. These results demonstrate that the TNTN sample exhibits superior electrochemical stability and corrosion resistance compared to the TNTV sample.

The impedance modulus (|Z|)–frequency curves given in Figure 6 illustrate the electrochemical application supporting the Nyquist diagrams presented in Figure 5. It is observed that both samples exhibit high impedance values in the low-frequency region. The impedance values between the TNTV and TNTN samples are quite close, but a regular decrease in impedance is observed for both samples with increasing frequency. This indicates that the system is controlled more by the resistance of the solution and the surface film properties in the high-frequency region. The higher charge transfer resistance observed for the TNTN sample in the Nyquist diagram is consistent with the relatively high impedance values in the low-frequency region. Overall, a combined analysis of the two graphs shows that the layered structure of the TNTN samples is more resistant to electrochemical pulses and that the system exhibits a more stable impedance performance in the low-frequency region.

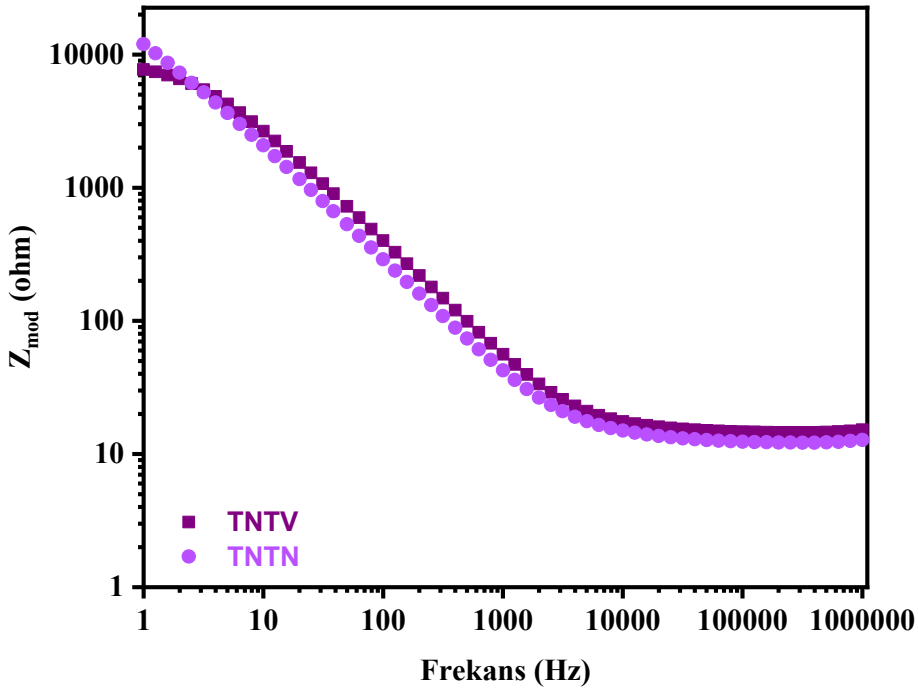

Figure 6. EIS Bode plot of TNTV and TNTN samples.

The electrochemical impedance spectroscopy (EIS) results presented in Figures 5 and 6 can be interpreted using the equivalent electrical circuit model shown in Figure 7. In this circuit, R_{soln} represents the ohmic resistance of the solution, while *C*c corresponds to the capacitive behavior of the coating or surface film. R_{po} denotes the pore resistance, reflecting the resistance against electrolyte penetration through the pores in the surface layer. Additionally, C_{cor} represents the double-layer capacitance or the capacitive

behavior at the corrosion interface, and R_{cor} corresponds to the charge transfer resistance, representing the resistance against corrosion reactions.

The semicircle diameters observed in the Nyquist diagram of Figure 5 are directly related to resistance components such as R_{cor} and R_{po}. An increase in the semicircle radius indicates a higher overall charge transfer resistance and a more resistant surface against electrochemical reactions. The impedance modulus–frequency curves (Bode plot) in Figure 6 further demonstrate that the high-frequency region is dominated by the effect of R_{soln}, whereas the low-frequency region is controlled by R_{cor} and C_{cor} components. Therefore, the combined analysis of both graphs confirms that the electrochemical behavior of the samples is well represented by the resistive and capacitive elements of the proposed equivalent circuit. In particular, the increase in impedance at low frequencies correlates with improved corrosion resistance. Electrochemical impedance spectroscopy (EIS) results reveal clear differences between the V-containing (TNTV) and Ni-containing (TNTN) alloys in 3.5% NaCl solution. The solution resistance values are relatively close for both samples, indicating similar electrolyte conditions. However, the charge transfer resistance (R_{cor}) of TNTN (14563.8 Ω) is significantly higher than that of TNTV (8628.4 Ω), suggesting that the Ni-added alloy exhibits superior corrosion resistance. Likewise, the pore resistance (R_{po}) of TNTN (18761.8 Ω) is markedly greater than that of TNTV (14.22 Ω), indicating the formation of a more protective and compact surface film on the TNTN alloy. In terms of capacitive behavior, both Ccor and Cc values are higher for TNTN, which can be associated with the presence of a thicker or more developed passive layer. On the other hand, the n value of TNTV is closer to unity, indicating a more ideal capacitive response and a relatively homogeneous surface. In contrast, the slightly lower n value of TNTN (0.8937) suggests increased surface heterogeneity. Overall, these findings indicate that while the TNTV alloy exhibits a more uniform surface behavior, the TNTN alloy provides significantly enhanced corrosion resistance due to the formation of a more stable and protective passive film. Studies on Ti–Nb–Ni and β-titanium based systems report very low corrosion current densities in corrosive environments, indicating strong passive film formation and enhanced corrosion resistance. For example, Folgueras et al. investigated the corrosion behavior of Ti–Nb–Ni foils in simulated environments and observed that the alloys exhibited strong passivation with relatively low corrosion current densities compared to conventional Ti alloys, consistent with improved electrochemical stability in aggressive media such as chloride-containing solutions[12]. An industrial Ti alloy, such as Ti-6Al-4V, typically exhibits more positive E_{cor}r and lower i_{corr} values in seawater tests, indicating high passive film stability [13].

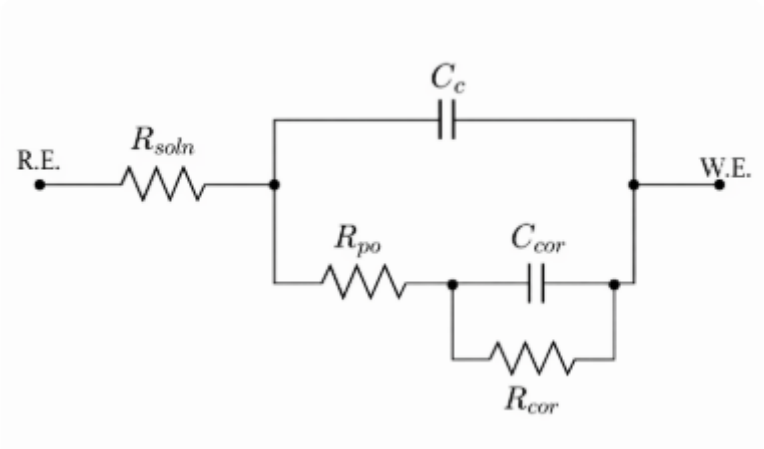

Figure 7. Impedance equivalent electrical circuits of TNTV and TNTN samples.

Table 3. Corrosion values obtained from Tafel analysis of the alloys.

Sample	E_{corr} (mV)	$\beta\alpha$ (mV/de)	β_c (mV/dec)	i_{corr} (μA.cm^{-2})	Corr. Rate (mm/year)
TNTV	-396.60	8.0285	6.428	0.248	8.252×10^{-3}
TNTN	-433.00	361.40	145.60	1.144	1.703×10^{-2}

Table 4. EIS values of TNTV and TNTN samples in % 3.5 NaCl.

Sample	R_{soln} (Ohm)	R_{cor} (Ohm)	R_{po}(Ohm)	Ccor (S.s^n)	n	C_c(S·s^m)	m
TNTV	14.51	8628.4	14.22	$4.62 \cdot 10^{-7}$	1	$8.64 \cdot 10^{-6}$	0.862
TNTN	12.47	14563.8	18761.8	$1.25 \cdot 10^{-5}$	0.8937	$1.27 \cdot 10^{-5}$	0.8694

Conclusion

In this study, the high-temperature oxidation behavior and electrochemical corrosion properties of TNTV and TNTN alloys were systematically investigated using TG analysis, isothermal oxidation tests, potentiodynamic polarization, and electrochemical impedance spectroscopy (EIS).

The results demonstrate that both alloys exhibit a clear temperature-dependent increase in oxidation rate constants, indicating accelerated oxidation kinetics at elevated temperatures. For the TNTV alloy, oxidation rate constants values increase from 0.125×10^{-2} to 1.120 mg·cm^{-2}·s^{-1} as the temperature rises from 500 to 1000 °C, while TNTN shows a similar trend with even higher oxidation rate constants values at elevated temperatures, reaching 1.473 mg·cm^{-2}·s^{-1} at 1000 °C. Moreover, the activation energy of TNTN is higher than that of TNTV, suggesting that the oxidation process in TNTN requires more energy to initiate but proceeds more rapidly once activated. Overall, despite its higher activation energy, the TNTN alloy exhibits greater oxidation rates at high temperatures, whereas TNTV demonstrates comparatively better oxidation resistance, particularly at lower and intermediate temperatures.

The Tafel analysis results presented clearly indicate that the electrochemical behaviour of the alloys differs significantly depending on their composition. The TNTV sample exhibits a much lower corrosion current density compared to TNTN, which corresponds to a substantially lower corrosion rate. This suggests that TNTV has superior corrosion resistance. Overall, the findings demonstrate that the TNTV alloy provides better corrosion performance, likely due to the formation of a more stable and protective passive layer on its surface.

EIS analyses indicate that, based on measurements in 3.5% NaCl, the TNTN sample exhibits markedly higher pore resistance and higher polarization resistance compared to TNTV; this suggests that the passive/film layer on TNTN is more resistant and that the electrochemical reaction kinetics are slowed, leading to a reduced corrosion current.

Author Contribution

Necdet Ercan: data analysis and writing; Esra Balci: performed the characterizations and writing, review; Fethi Dağdelen: Project administration Conceptualization, Review. This article is derived from Necdet Ercan's thesis.

Conflict of Interests

Authors declare that there is no financial and non-financial conflict of interests.

References

[1] E. Balci, F. Dagdelen, I.N. Qader, M. Kok, Effects of substituting Nb with V on thermal analysis and biocompatibility assessment of quaternary NiTiNbV SMA, The European Physical Journal Plus 136(2) (2021) 145.

[2] E. Dong, W. Yu, Q. Cai, L. Cheng, J. Shi, High-temperature oxidation kinetics and behavior of Ti–6Al–4V alloy, Oxidation of Metals 88(5) (2017) 719-732.

[3] P. A. Ibrahim , S.A. Baiz , S.S. Mohammed , E. Balci, F. Dagdelen, Influence of Heat Treatment Temperature on Phase Transformation Behavior and Mechanical Performance of $Ti_{50}Ni_{39}Zr_{10}Nb_1$ SMA, Physics and Astronomy Reports, 2026,4(1),1–8, DOI :10.26650/PAR.2026.00002.

[4] E. Balcı, F. Dagdelen, Thermal, structural properties and potential dynamic corrosion study of Ti-27Ni-21Nb-2Ta SMA, Iranian Journal of Science and Technology, Transactions A: Science 46(1) (2022) 353-359.

[5] E. Balci, I. Somunkiran, E. Ercan, F. Dagdelen, Y. Aydogdu, A study on isothermal oxidation kinetics using thermogravimetric method of TiNiNb shape memory alloys, Journal of Thermal Analysis and Calorimetry 148(24) (2023) 14253-14260.

[6] S. Mohammed, E. Balci, F. Dagdelen, S. Saydam, Comparison of thermodynamic parameters and corrosion behaviors of Ti50Ni25Nb25 and Ti50Ni25Ta25 shape memory alloys, Physics of Metals and Metallography 123(14) (2022) 1427-1435.

[7] E. Balci, F. Dagdelen, The comparison of TiNiNbTa and TiNiNbV SMAs in terms of corrosion behavior, microhardness, thermal and structural properties, Journal of Thermal Analysis and Calorimetry 147(20) (2022) 10943-10949.

[8] F. Dagdelen, E. Ercan, The surface oxidation behavior of Ni–45.16% Ti shape memory alloys at different temperatures, Journal of Thermal Analysis and Calorimetry 115(1) (2014) 561-565.

[9] E. Dong, W. Yu, Q. Cai, L. Cheng, J. Shi, High-temperature oxidation kinetics and behavior of Ti–6Al–4V alloy, Oxidation of Metals 88 (2017) 719-732.

[10] R.R. Wang, K.K. Fung, Oxidation behavior of surface-modified titanium for titanium-ceramic restorations, The Journal of prosthetic dentistry 77(4) (1997) 423-434.

[11] E. Balci, F. Dagdelen, S. Mohammed, E. Ercan, Corrosion behavior and thermal cycle stability of TiNiTa shape memory alloy, Journal of Thermal Analysis and Calorimetry 147(24) (2022) 14953-14960.

[12] H. Zhu, X. Wang, W. Meng, P. Ming, F. Kong, Corrosion behavior of Ti-Nb-Ni foil as bipolar plates substrate in simulated PEMFC solution: Effects of fluoride concentration and temperature, Fuel 362 (2024) 130823.

[13] L. Vrsalović, S. Gudić, A. Talijančić, J. Jakić, J. Krolo, I. Danaee, Corrosion behavior of Ti and Ti6Al4V alloy in brackish water, seawater, and seawater bittern, Corrosion and materials degradation 5(4) (2024) 641-656.